Available online at www.sciencedirect.com
ScienceDirect
Journal of Colloid and Interface Science 322 (2008) 660–668
JOURNAL OF Colloid and Interface Science
www.elsevier.com/locate/jcis

Modeling the surface charge evolution of spherical nanoparticles by considering dielectric discontinuity effects at the solid/electrolyte solution interface

Marianne Seijo, Serge Ulrich, Montserrat Filella, Jacques Buffle, Serge Stoll *

CABE (Analytical and Biophysical Environmental Chemistry), Department of Inorganic, Analytical and Applied Chemistry, University of Geneva, Sciences II, 30 quai E. Ansermet, CH-1211 Geneva 4, Switzerland

Received 25 January 2008; accepted 22 February 2008

Available online 2 April 2008

Abstract

It is well known that the electrostatic repulsions between charges on neighboring sites decrease the effective charge at the surface of a charged nanoparticle (NP). However, the situation is more complex close to a dielectric discontinuity, since charged sites are interacting not only with their neighbors but also with their own image charges and the image charges of all neighbors. Titrating site positions, solution ionic concentration, dielectric discontinuity effects, and surface charge variations with pH are investigated here using a grand canonical Monte Carlo method. A Tanford and Kirkwood approach is used to calculate the interaction potentials between the discrete charged sites. Homogeneous, heterogeneous, and patch site distributions are considered to reproduce the various titrating site distributions at the solid/solution interface of spherical NPs. By considering Coulomb, salt, and image charges effects, results show that for different ionic concentrations, modifications of the dielectric constant of NPs having homogeneous and heterogeneous site distributions have little effect on their charging process. Thus, the reaction field, due to the presence of image charges, fully counterbalances the Coulomb interactions. This is not the case for patch distributions, where Coulomb interactions are not completely counterbalanced by the reaction field. Application of the present model to pyrogenic silica is also performed and comparison is made with published experimental data of titration curves at various ionic concentrations.

Keywords: Nanoparticle surface charge; Nanoparticle titration curves; Monte Carlo simulations; Tanford and Kirkwood model; Dielectric discontinuity

1. Introduction

Nanoparticle synthesis and production are now a fast growing area of research and nanotechnology development. Due to their sizes, nanoparticles (NPs) have physicochemical properties which differ from their identical larger size counterparts. In particular, their high specific surface areas make them very reactive, catalytic, and mobile. However, NP properties are largely controlled by their surface charge, which will change as a function of the physicochemical dispersion media conditions (pH, concentration of dissolved ions, etc.). Surface charge will then affect NP adsorption, reactivity, and adsorption on biomaterials. Surface charge can also have a significant impact on both their fate and their potential harmful properties, since NPs can occur as either aggregated or dispersed material according to prevailing chemical conditions. Aggregates of NPs will sediment and become immobilized, while dispersed NPs will diffuse in soils/sediments/waters, and thus will be more mobile and more bioavailable.

The overall charge of NPs is determined by the probability of each surface site, or functional group, to be ionized. Surface charge is mainly due to proton-binding reactions. This probability depends on chemical equilibria that can be tuned by varying the pH or ionic concentration of the solution. In contrast to dilute solutions of isolated titrating sites, at the NP surface, each site is influenced by the presence of all other sites. As a result, mutual electrostatic repulsions between charges are expected to limit the effective charge of the NPs [1–3]. A few models are commonly used to describe charged interfaces, such as the 2-

* Corresponding author.
E-mail address: serge.stoll@cabe.unige.ch (S. Stoll).

0021-9797/$ – see front matter
doi:10.1016/j.jcis.2008.02.027

pKa [4], Music [5], and CD-Music models [6], which differ in the number of possible proton binding reactions and the value of charges on the surfaces. Moreover, we can expect that the situation is even more complex when a dielectric discontinuity is considered at the NP–solution interface, since the charge of each site is then interacting not only with its neighbors but also with its own image charge and the image charges of all the neighbors. Due to the many-body nature of this problem, as well as the long-range nature of the electrostatic interactions, exact analytical solutions for the calculation of the NPs average charge as a function of pH by considering the presence of a dielectric discontinuity are generally not known. In addition, due to surface defects or the additional heterogeneity induced by adsorbed molecules, it is generally accepted that interfacial site distributions are heterogeneous. As a result, interface heterogeneity results in variation in proton affinity among surface sites [7,8].

When a dielectric discontinuity is considered, the charging process of an ionizable water–solid interface is usually influenced by the geometry of the interface which can be planar or spherical. Borkovec [9] investigated the behavior of a discrete-charge Ising model of ionizable water–solid interface using Monte Carlo simulations. Site–site interaction potentials were calculated within the linearized Poisson–Boltzmann approximation [10]. Ionizable sites were approximated by point charges buried in a solid of fixed dielectric constant (set to 3) at a distance from the planar interface to the electrolyte solution of dielectric constant equal to 80. It was concluded that for a planar ionizable interface, mean field approximations inherent to all surface complexation models are sound, the basic reason being related to the long-range character of the site–site interaction potentials.

The charging process of a weak linear and negatively charged polymer chain in the vicinity of a planar surface was studied by Netz [11]. It was shown that close to a dielectric discontinuity when the dielectric constant of the media, within the polymer, is higher than the other side of the dielectric discontinuity, the image charges influence the dissociation equilibrium by (i) decreasing the total charge of the polymer and (ii) repulsing the polymer from the interface. On the other hand, at low dielectric constant values within the polymer, the polymer effective charge was shown to increase and the polymer was attracted by the surface.

When spherical interfaces are considered, the resulting interaction potential between charged sites are notoriously difficult to solve because of curvature effects. To solve such a problem, the Tanford and Kirwood (TK) approach can be used. The general potential of a spherical entity having a discrete site distribution was developed by Tanford and Kirkwood [12,13]. General equations for impenetrable spheres were derived and mainly applied to globular proteins to achieve a detailed evaluation of the proton binding and anisotropy of proton fluctuations in proteins [14–16]. The TK model yields good agreement between most calculated and observed pK_a values in proteins [17–19]. Using the TK model, Linse [20] investigated the effects of the image charges on the properties of a spherical electrical double layer around a micelle by considering explicit ions. It was concluded that the surface polarization reduces the counterion accumulation at the surface as well as the angular fluctuation of the counterion distribution from spherical symmetry. Such effects were found important for divalent counterions or at low surface charge densities.

In this paper, using simultaneously the Tanford and Kirwood approach and Monte Carlo simulations, we investigate the charging behavior of an isolated spherical NP by considering the presence of a dielectric discontinuity with the solution. Effects of surface site distributions and effects related to the presence of salt in the solution are also investigated. A systematic approach is used and a comparison is made with experimental data to check how well the ionic concentration effect on the charging behavior is predicted by this approach. The many-body nature of the problem is solved using Monte Carlo simulations, which are performed according to the Metropolis algorithm [21]. To obtain equilibrium between all the charged configurations of the NP at a given pH, simulations have been performed in the grand canonical ensemble, where the chemical potential, μ, volume, V, and temperature, T, are fixed. Ions in solution are treated implicitly, due to the important computational time required when the focus is made on the charging behavior of explicit sites by adjusting pH, ionic concentration, and dielectric discontinuity.

2. Model description

2.1. Interaction potentials

Calculations of the interaction potentials between charged sites are performed according to the Tanford model [12]. The NP is considered as a sphere in an infinitely diluted aqueous electrolyte solution (isolated sphere). The NP is impenetrable to the ionic species and the solvent molecules. To take into account the NP/solution dielectric discontinuity, the relative permittivity ε_c of the NP can be adjusted to be different from the dielectric constant of the surrounding water ε_w (Fig. 1).

Salt ions are not represented explicitly. Nevertheless, the energy associated with the anisotropic distribution of charge positions at the NP surface interacting with ions is considered in the potential (see Eq. (4) below). Since mobile ions in the solvent have finite radius, the NP with radius R_c (region I) is surrounded by a small exclusion layer, which is impenetrable to ionic species and expected to represent the Stern layer (region II). In this region, the relative permittivity is arbitrarily set to ε_w and the ionic concentration to zero. The layer thickness, l_S, which can be adjusted in the model, is equal to the dimension of the radius of the smallest salt ion in the solution. In the first part of the present work, l_S is fixed to 0.5 Å but it can be adjusted as a function of the chemical nature of ionic species in solution. In the third region, ionic species and solvent are represented as a structureless continuum with relative permittivity ε_w and ionic concentration C_i.

Titrating sites are represented by fixed point charges located at a distance of 0.5 Å from the dielectric discontinuity ($r = R_c - 0.5$ Å, Fig. 1). The Tanford–Kirkwood theory is used to calculate the electrostatic energy by considering the discrete

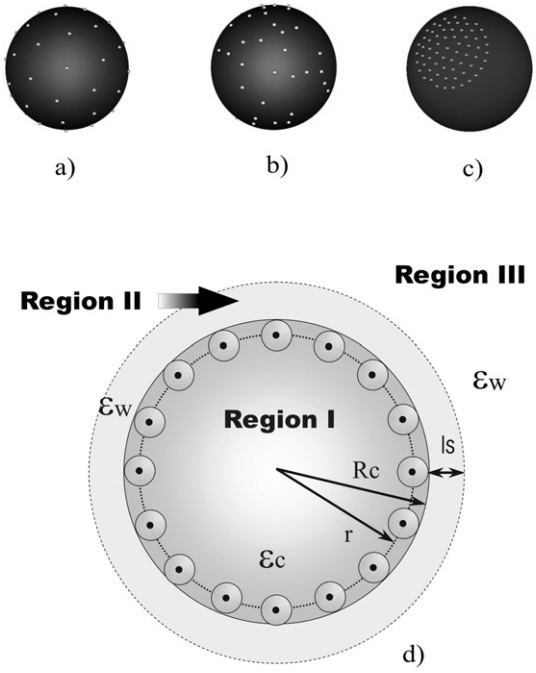

Fig. 1. Configurations of the NP surface discrete charge distributions: (a) homogeneous, (b) heterogeneous, and (c) one-patch distribution. (d) Schematic representation of the NP model. This is represented by a sphere of radius R_c (region I) surrounded by two regions: The Stern layer (region II) of thickness l_S and the outer solution (region III). Titrating sites are represented by fixed point charges located within the spherical dielectric at a distance r from the center of the sphere.

charge distribution, the dielectric discontinuity, and the influence of an ionic distribution in the solution.

Two ionized sites of charge z_i and z_j located at a radial position r, separated by a distance r_{ij} with an angle θ_{ij} (with $\cos\theta_{ij} = 1 - r_{ij}^2/2r^2$), contribute to an electrostatic potential energy (in $k_B T$ units) given by

$$E_{el} = \frac{z_i z_j e^2}{4\pi\varepsilon_0 k_B T}(A_{ij} - B_{ij} - C_{ij}), \tag{1}$$

where e represents the elementary charge and ε_0 the vacuum permittivity. A_{ij} represents the direct Coulomb contribution and is given by

$$A_{ij} = \frac{1}{r_{ij}\varepsilon_c}, \tag{2}$$

whereas B_{ij} represents the reaction field contribution of the electrostatic potential energy (due to the presence of dielectric discontinuity) and is given by

$$B_{ij} = \frac{1}{\varepsilon_c R_c}\sum_{n=0}^{n_{max}} \frac{(\varepsilon_w - \varepsilon_c)P_n^0(\cos\theta_{ij})}{(\varepsilon_w + \varepsilon_c(n/n+1))}\left(\frac{r^2}{R_c^2}\right)^n, \tag{3}$$

where n_{max} is the maximum number of terms included in the sum and P_n^0 is the ordinary Legendre polynomial of order n. It should be noted that a large number of terms are needed for the ordinary Legendre polynomial to converge. This limits from a computational point of view the number of sites in the model. With sites located at 0.5 Å from the dielectric discontinuity, an accuracy of about 10^{-5} with $n_{max} = 500$ is achieved.

C_{ij} represents the interaction of charges with the salt ions in the solvent, i.e., the ionic concentration effect. C_{ij} is given by

$$\begin{aligned} C_{ij} = \frac{1}{\varepsilon_w(R_c + l_S)}\Bigg[& \frac{\kappa(R_c + l_S)}{1 + \kappa(R_c + l_S)} \\ & + x^2 \sum_{n=1}^{n_{max}} \left(\frac{2n+1}{2n-1}\left(\frac{\varepsilon_w}{(n+1)\varepsilon_w + n\varepsilon_c}\right)^2 \left(\frac{r^2}{(R_c + l_S)^2}\right)^n \right. \\ & \times P_n^0(\cos\theta_{ij}) \\ & \times \left(\left(\frac{K_{n+1}(x)}{K_{n-1}(x)}\right) + \frac{n(\varepsilon_w - \varepsilon_c)}{\varepsilon_w(n+1) + n\varepsilon_c}\left(\frac{R_c}{R_c + l_S}\right)^{2n+1} \right. \\ & \left.\left. \times \frac{[\kappa(R_c + l_S)]^2}{4n^2 - 1}\right)^{-1}\right)\Bigg], \end{aligned} \tag{4}$$

where N_A represents the Avogadro number and κ is the inverse Debye screening length [m^{-1}], defined by

$$\kappa = \sqrt{1000 e^2 N_A \sum_i \frac{z_i^2 C_i}{\varepsilon_0 \varepsilon_w k_B T}}. \tag{5}$$

C_i represents the ionic concentration and $x = \kappa(R_c + l_S)$. The auxiliary functions are defined as

$$K_n(x) = \sum_{s=0}^{n} \frac{2^s n!(2n-s)!}{s!(2n)!(n-s)!}x^s. \tag{6}$$

Here C_{ij} vanishes to zero when $\kappa = 0$, i.e., in the absence of salt.

To validate our computer code, theoretical results for isolated sites and results obtained by Tanford [12] and Orttung [14] with simple models were calculated and reproduced correctly.

2.2. Chemical equilibria

For a monoprotic chemical reaction in an aqueous medium, the acid–base properties of an isolated site are described by the Henderson–Hasselbalch equation [22,23]:

$$\mathrm{pH} = \mathrm{p}K_{ai}^0 \pm \log_{10}\left(\frac{1-\alpha}{\alpha}\right). \tag{7}$$

Here the plus sign is used to consider the degree of proton association (or degree of protonation, α_p) and the minus sign corresponds to the degree of proton dissociation (α_d). K_{ai}^0 represents the intrinsic dissociation constant for the monoprotic reaction, K_{a1}^0 or K_{a2}^0, and is defined as

$$\left(\mathrm{Site} - \mathrm{H}_2^+\right) \overset{K_{a1}^0}{\rightleftarrows} (\mathrm{Site} - \mathrm{H}) + \mathrm{H}^+, \tag{8}$$

$$(\mathrm{Site} - \mathrm{H}) \overset{K_{a2}^0}{\rightleftarrows} (\mathrm{Site}^-) + \mathrm{H}^+. \tag{9}$$

For a diprotic chemical reaction, the Henderson–Hasselbalch equation may be reformulated to give

$$2\mathrm{pH} = \mathrm{p}K_{a1}^0 + \mathrm{p}K_{a2}^0 + \log_{10}\left(\frac{1-\alpha_p}{\alpha_p}\right). \tag{10}$$

Table 1
Chemical equilibria and associated energy changes used in the Monte Carlo simulations

Initial charge state	Possible charge state	Acid/base chemical reaction	Change in energy, ΔE (in $k_B T$ units)
0	+1	$(\text{Site}-\text{H}) + \text{H}^+ \overset{1/K^0_{a1}}{\rightleftharpoons} (\text{Site}-\text{H}_2^+)$	$\Delta E = \Delta E_{\text{electrostatic}} + (\text{pH} - \text{p}K^0_{a1})\ln(10)$
	−1	$(\text{Site}-\text{H}) \overset{K^0_{a2}}{\rightleftharpoons} \text{Site}^- + \text{H}^+$	$\Delta E = \Delta E_{\text{electrostatic}} - (\text{pH} - \text{p}K^0_{a2})\ln(10)$
+1	0	$(\text{Site}-\text{H}_2^+) \overset{K^0_{a1}}{\rightleftharpoons} (\text{Site}-\text{H}) + \text{H}^+$	$\Delta E = \Delta E_{\text{electrostatic}} - (\text{pH} - \text{p}K^0_{a1})\ln(10)$
	−1	$(\text{Site}-\text{H}_2^+) \overset{K^0_{a1}K^0_{a2}}{\rightleftharpoons} \text{Site}^- + 2\text{H}^+$	$\Delta E = \Delta E_{\text{electrostatic}} - (2\text{pH} - \text{p}K^0_{a1} - \text{p}K^0_{a2})\ln(10)$
−1	0	$\text{Site}^- + \text{H}^+ \overset{1/K^0_{a2}}{\rightleftharpoons} (\text{Site}-\text{H})$	$\Delta E = \Delta E_{\text{electrostatic}} + (\text{pH} - \text{p}K^0_{a2})\ln(10)$
	+1	$\text{Site}^- + 2\text{H}^+ \overset{1/(K^0_{a1}K^0_{a2})}{\rightleftharpoons} (\text{Site}-\text{H}_2^+)$	$\Delta E = \Delta E_{\text{electrostatic}} + (2\text{pH} - \text{p}K^0_{a1} - \text{p}K^0_{a2})\ln(10)$

For a monoprotic chemical dissociation, Eq. (7) can be expressed as

$$\text{pH} = \text{p}K^0_a + \log_{10}\left(\frac{1-\alpha_p}{\alpha_p}\right) + \frac{1}{k_B T \ln(10)}\frac{\partial \overline{U}(N_i)}{\partial N_i}, \qquad (11)$$

where N_i represents the number of ionized sites and $\overline{U}(N_i)$ the average NP electrostatic energy (with N_i ionized sites).

For a diprotic chemical dissociation, Eq. (7) then becomes

$$2\text{pH} = \text{p}K^0_{a1} + \text{p}K^0_{a2} + \log_{10}\left(\frac{1-\alpha_p}{\alpha_p}\right) + \frac{1}{k_B T \ln(10)}\frac{\partial \overline{U}(N_p, N_0)}{\partial N_0}, \qquad (12)$$

where N_0 and N_p are the number of unprotonated and protonated sites respectively.

2.3. Monte Carlo Metropolis and statistical ensemble

To explore the charge amount and site distribution configuration space, Monte Carlo simulations are performed according to the Metropolis algorithm [21]. Since the NP has N ionizable sites, 3^N possible charge states are possible. For each Monte Carlo step, a site is chosen at random and its charge state is changed randomly. Two new charge states are then possible among the three charge states. Then each acid–base reaction is accepted or not by considering the Metropolis selection criterion. The acceptance criterion is sensitive to the value of the energy variation, ΔE, during the protonation and deprotonation processes as defined in Table 1. Simulations are performed in the grand canonical ensemble, which has been successfully used to study energetically heterogeneous metal oxide/electrolyte interfaces [24,25].

2.4. Spatial configuration of surface discrete charge distribution

Three spatial distributions of sites are considered: (i) a homogeneous discrete site distribution (Fig. 1a), (ii) a random heterogeneous discrete site distribution (Fig. 1b), and (iii) a discrete distribution where sites are confined in patches (Fig. 1c).

Table 2
Details of the patch distribution positions at the NP surface

	1 patch	2 patches	3 patches
	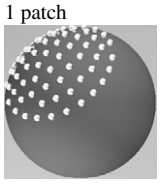	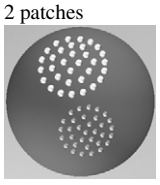	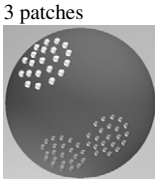
Radius of patches [nm]	11.32	8.0	6.5
Number of sites per patch	66	33	22
Coordinates of the centers of patches, with θ and φ defined as in Ref. [8]	*P1*: $\theta_1 = \pi/2$, $\varphi_1 = 0$	*P1*: $\theta_1 = \pi/2$, $\varphi_1 = 0$ *P2*: $\theta_2 = -\pi/2$, $\varphi_2 = 0$	*P1*: $\theta_1 = \pi/2$, $\varphi_1 = 0$ *P2*: $\theta_2 = -\pi/2$, $\varphi_2 = 0$ *P3*: $\theta_3 = \pi/4$, $\varphi_3 = 0$

Note. The total number of sites is equal to 66 in all cases. These 66 sites are homogeneously distributed in the patches. The patch radius is calculated in order to achieve the same local density per patch, equal to 0.16 sites/nm^2.

A sphere with an arbitrary radius of 20 nm is considered. The sizes and positions of the patches are detailed in Table 2. In order to fit the Debye–Hückel limitation imposed by the Tanford and Kirkwood model, hence avoiding high-charge-density distributions, 66 titrating sites are considered, corresponding to a maximum surface charge equal to 2.1 mC m^{-2}. Under such conditions, no counterion condensation is expected to occur, due to the fact that the maximal surface charge of 2.1 mC m^{-2} is lower than the critical surface charge σ_{crit} calculated with Manning's equation [26,27]. Indeed, when $C_i = 10^{-3}$ mol L^{-1}, $\sigma_{crit} = 14.6$ mC m^{-2}, whereas when $C_i = 10^{-2}$ mol L^{-1}, $\sigma_{crit} = 20.0$ mC m^{-2}. Equilibration times are obtained after 1000 Monte Carlo steps prior to a production period in which a representative statistical ensemble is obtained. Production times are then performed using 20,000 Monte Carlo steps. To achieve full titration curves, equilibration and production times are performed for each pH value.

Titrating curves are systematically compared with the corresponding ideal cases, i.e., in absence of electrostatic inter-

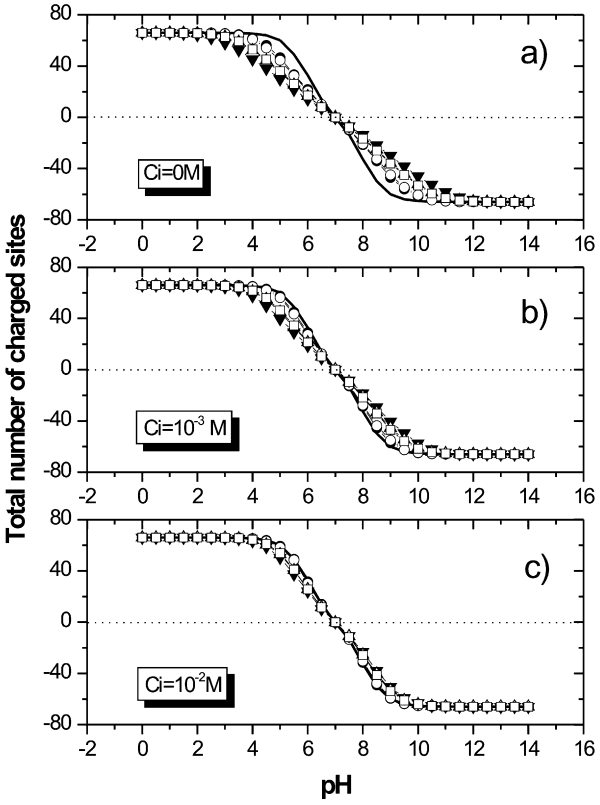

Fig. 2. NP titration curves. Effects of pH, surface site distribution and ionic strength are presented. No dielectric discontinuity is considered here ($\varepsilon_c = \varepsilon_w = 78.54$). $pK^0_{a1} = 6.0$, $pK^0_{a2} = 8.0$. The corresponding ideal case is represented by a continuous line. (●) Homogeneous site distribution, (○) heterogeneous site distribution, (□) three-patch distribution, (△) two-patch distribution, (▼) one-patch distribution.

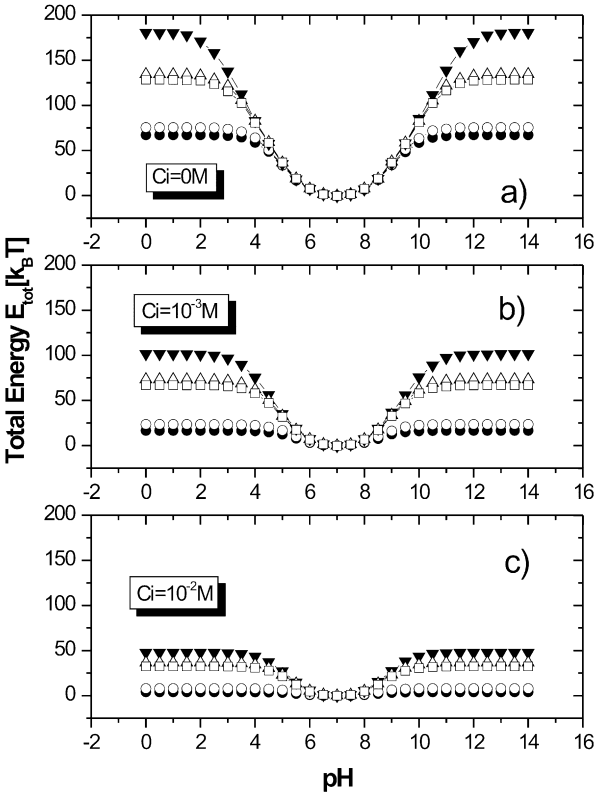

Fig. 3. Variations of the total energy for the different site distributions as a function of the pH with $\varepsilon_c = \varepsilon_w = 78.54$. (●) Homogeneous site distribution, (○) heterogeneous site distribution, (□) three-patch distribution, (△) two-patch distribution, (▼) one-patch distribution.

actions between sites. The relative concentrations of deprotonated, neutral, and protonated sites, P_{-1}, P_0, and P_1, are given by

$$P_{-1} = \frac{[\text{Site}^-]}{[\text{Site}^-] + [\text{Site} - \text{H}] + [\text{Site} - \text{H}_2^+]} = \frac{1}{1 + (K^0_{a2})^{-1}[\text{H}^+] + (K^0_{a1}K^0_{a2})^{-1}[\text{H}^+]^2}, \quad (13)$$

$$P_0 = \frac{[\text{Site} - \text{H}]}{[\text{Site}^-] + [\text{Site} - \text{H}] + [\text{Site} - \text{H}_2^+]} = \frac{(K^0_{a2})^{-1}[\text{H}^+]}{1 + (K^0_{a2})^{-1}[\text{H}^+] + (K^0_{a1}K^0_{a2})^{-1}[\text{H}^+]^2}, \quad (14)$$

$$P_1 = \frac{[\text{Site} - \text{H}_2^+]}{[\text{Site}^-] + [\text{Site} - \text{H}] + [\text{Site} - \text{H}_2^+]} = \frac{(K^0_{a1}K^0_{a2})^{-1}[\text{H}^+]^2}{1 + (K^0_{a2})^{-1}[\text{H}^+] + (K^0_{a1}K^0_{a2})^{-1}[\text{H}^+]^2}. \quad (15)$$

Two pK_a values are used here with $pK^0_{a1} = 6$ and $pK^0_{a2} = 8$. These values are here arbitrarily fixed but can be freely adjusted in the present model.

3. Results and discussion

3.1. Influence of the ionic concentration and surface site distribution in the absence of dielectric discontinuity

In order to explore first the influence of the different site distributions and ionic concentrations on the NP charging process, simulations are carried out at $C_i = 0$, 10^{-3}, and 10^{-2} mol L^{-1}. Temperature is set to 298 K, and $\varepsilon_c = \varepsilon_w = 78.54$ (no dielectric discontinuity). The NP surface charge variation is presented in Figs. 2a, 2b, and 2c as a function of the solution pH and for the different ionic concentrations. It is shown that the nonideal cases exhibit fewer surface charges than the ideal case (continuous line) due to the presence of short- and long-range electrostatic repulsions between charged sites, which makes difficult a further increase of the surface charge density. By increasing the ionic concentration, homogeneous, heterogeneous, and patch distributions are moving to the ideal case due to the screening of long-range electrostatic interactions between sites. The effect of the surface site distribution is clearly shown here. The heterogeneous distribution and the patch distributions are significantly less charged than the homogeneous distribution, the one-patch distribution being the most difficult to ionize due to the large number of short-range interactions in this configuration. As expected, the point of zero charge is observed when $\text{pH} = (1/2)(pK^0_{a1} + pK^0_{a2})$.

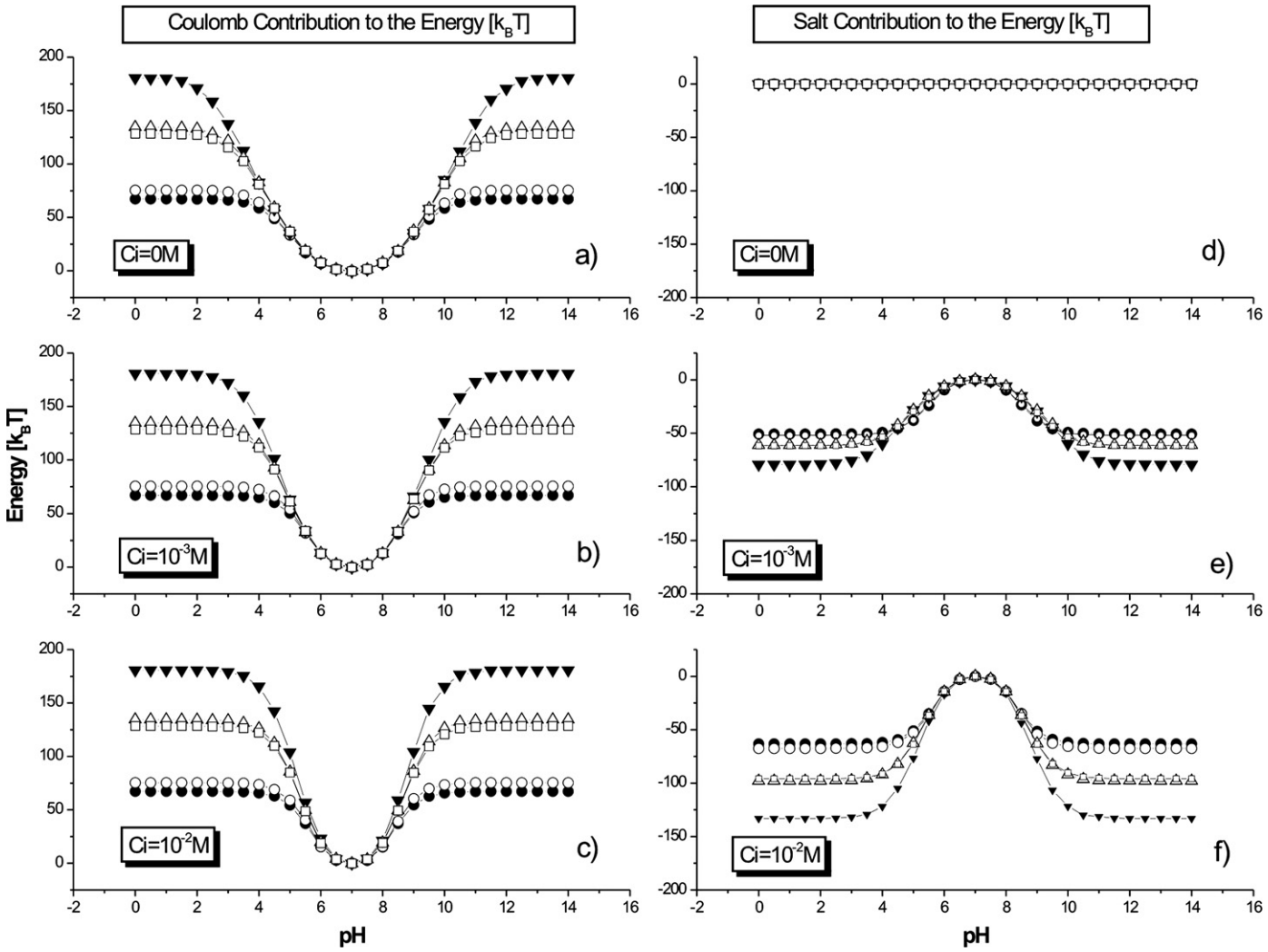

Fig. 4. Details of the Coulomb and salt contributions to the energy versus pH, ionic strength ($\varepsilon_c = \varepsilon_w = 78.54$). (●) Homogeneous site distribution, (○) heterogeneous site distribution, (□) three-patch distribution, (△) two-patch distribution, (▼) one-patch distribution.

In Figs. 3a, 3b, and 3c the total energy E_{tot} of the NP (i.e., the sum of the Coulomb and salt contribution) is represented as a function of pH at the different ionic concentrations. It is observed that by increasing the ionic concentration, an overall decrease of the total energy is observed, in agreement with the increase of the surface charge values (Fig. 2). The presence of salt in solution clearly decreases the intensity of the electrostatic interactions between charged sites and promotes the NP surface charging process. The influence of the surface site distribution on E_{tot} is clear: the one-patch distribution has the highest energy whereas the homogeneous distribution has the lowest one.

To get insight into the relative contributions of the Coulomb and salt effects, they have been represented in Fig. 4 as a function of the pH and for various salt concentrations. It should be noted that the Coulomb energy has a positive contribution whereas the salt contribution to the energy is negative (stabilization effect). At low ionic concentration the Coulomb interactions make the most important contributions to the total energy. Hence Coulomb interactions mainly control the charging process. Considering the salt effect, at low ionic concentration, the first term of Eq. (4) is predominant and independent of the location of charges. Mobile salt ions in solution are assumed to be sufficiently far from the surface [13]. Hence, the salt contribution is less sensitive to the charged site distribution than Coulomb interactions. When the ionic concentration increases, the first term of the summation in Eq. (4) (i.e., the isotropic term of the salt part of energy) does not fully control the ionic concentration effect yet. The major contribution to the C_{ij} value comes from terms with $\cos\theta$ close to unity, and thus, from smallest distances between charges, since salt ions are confined close to the charged sites. As a result, the ionic concentration contribution to the total energy becomes non-negligible, site-distribution-related, and of the same order of magnitude than Coulomb interactions at relatively high salt concentration (10^{-2} mol L^{-1}). In particular, when many charges are close to each other, such as in the one-patch distribution, the salt contribution is important.

During charging processes, the distribution of charges at the surface of the NP is expected to be relatively homogeneous to reduce the electrostatic energy (even if the site distribution is not homogeneous). This behavior was observed for the ho-

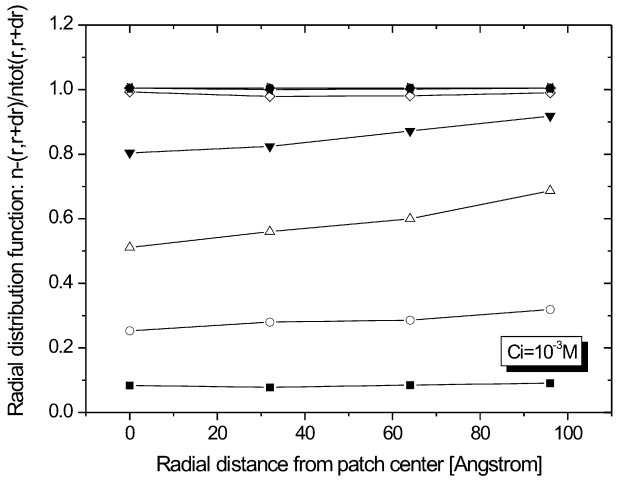

Fig. 5. Variation of the negatively charged sites density at a distance r to $r + dr$ (radial distribution function) as a function of the distance r from the center of the patch, with (■) pH 7, (○) pH 8, (△) pH 9, (▼) pH 10, (◇) pH 11, (◄) pH 12, (▷) pH 14.

mogeneous and heterogeneous site distributions but not for the patch distribution. To get insight into the charge distribution within the patches, we investigated the radial charge distribution inside one patch at a given ionic concentration and for different pH values. As shown in Fig. 5, when $C_i = 10^{-3}$ mol L^{-1}, finite size effects are observed; charge depletion is obtained at the centers of the patches for intermediate pH values, i.e., when the degree of ionization is less than one. When the pH is increased, charges accumulate at the perimeter, where site density is lower. With further increase, the pH charges also accumulate at the center of the patch to achieve a homogeneous radial distribution of charged sites. Such finite size effects disappear with increasingly high ionic concentration due to the screening of the repulsive charge–charge electrostatic repulsions.

3.2. *Influence of the ionic concentration and surface site distribution in the presence of dielectric discontinuity*

To explore the influence of both the dielectric discontinuity and the ionic concentration on the NP charging process, simulations are carried out with $\varepsilon_w = 78.54$, $C_i = 0$, 10^{-3}, and 10^{-2} mol L^{-1}, and $\varepsilon_c = 2$, 30, 78.54, and 114. The pH value is set to 9.25 to consider a significant number of surface charges. As illustrated in Fig. 6a, when $C_i = 0$ mol L^{-1}, the dielectric discontinuity has little effect on the NP ionization degree for the homogeneous and heterogeneous distributions. For such site distributions, dielectric constant changes inside the NP are counterbalanced by the presence of the reaction field, in particular when the NP dielectric constant is decreased (as shown in Table 3, where the corresponding energies of the reaction field and Coulomb interactions are given).

In contrast, patch distributions are more influenced by ε_c variations. By decreasing ε_c the degree of ionization is clearly reduced due to the increase of the importance of the Coulomb electrostatic repulsions. Here the reaction field, which induces image charges of opposite sign within the NP ($\varepsilon_c < \varepsilon_w$), is not strong enough to fully counterbalance the Coulomb interactions. On the other hand, when the NP dielectric constant is greater than the water dielectric constant value, ionization is promoted because of the decrease of the intensity of Coulomb interactions. Here the reaction field, which induces image charges of the same sign ($\varepsilon_c > \varepsilon_w$), makes a positive but small contribution to the total energy.

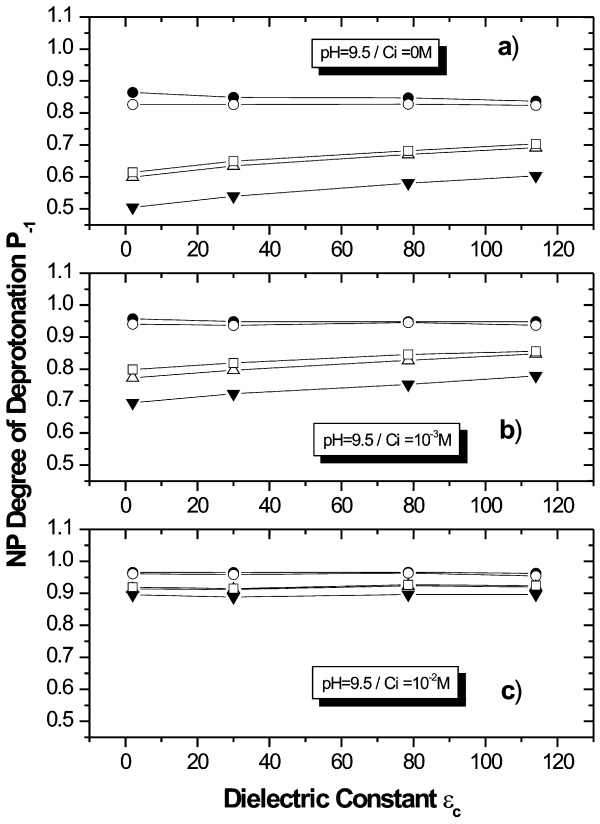

Fig. 6. Degree of deprotonation P_{-1} at pH 9.5 as a function of the NP dielectric constant ε_c for different site distributions and various ionic concentrations. (●) Homogeneous site distribution, (○, □) three-patch distribution, (△) two-patch distribution, (▼) one-patch distribution.

By increasing the ionic concentration as shown in Figs. 6b and 6c, screening of the charge repulsions promotes the degree of ionization in all cases (homogeneous, heterogeneous, and patch distributions) and reduces the dielectric discontinuity effects. In particular, at high ionic concentration, the influence of the NP dielectric change when patch distributions are considered is cancelled (Fig. 6c).

4. Comparison with experimental data

In the studies of Gilson and Honig [28] comparisons between different models were performed. The authors conclude that TK model can serve as a convenient approximation to the full Poisson–Boltzmann solutions, at least in the case of globular proteins, but also when charge densities exhibit high values. To validate the description of the TK model and Monte Carlo approach on the titration behavior of spherical and relatively highly charged NPs, the charging process of pyrogenic silica was calculated and compared with experimental data that were kindly provided by Thomas and Prélot [29].

Table 3
Details of the Coulomb, salt, and reaction field contributions to the energy (k_BT units) versus ionic strength and dielectric constant variation ε_c of the NP (pH 9.5)

ε_c	Homogeneous-site distribution, $C_i = 0$ M				One-patch-site distribution, $C_i = 0$ M			
	$E_{Coulomb}$	$E_{reaction}$	E_{salt}	E_{tot}	$E_{Coulomb}$	$E_{reaction}$	E_{salt}	E_{tot}
2	1973.34	−1928.13	0	45.1945	1656.54	−1602.48	0	54.0653
30	126.697	−80.6883	0	46.0057	128.213	−71.7233	0	56.4894
78	48.2584	0	0	48.2584	58.116	0	0	58.116
114	32.3979	15.6633	0	48.0612	43.3196	+14.7111	0	58.0306
	Homogeneous-site distribution, $C_i = 10^{-2}$ M				One-patch-site distribution, $C_i = 10^{-2}$ M			
	$E_{Coulomb}$	$E_{reaction}$	E_{salt}	E_{tot}	$E_{Coulomb}$	$E_{reaction}$	E_{salt}	E_{tot}
30	2463.25	−2406.78	−55.326	1.1094	5655.03	−5467.99	−150.685	36.3557
78	164.067	−104.489	−57.1873	2.40057	372.151	−207.301	−127.283	37.5668
114	62.772	0	−58.9697	3.81105	144.724	0	−106.575	38.1482

These authors investigated the features of the charging curves of pyrogenic silica/$NaClO_4$ electrolytic solution interfaces by performing potentiometric titrations at various ionic concentrations. All parameters used in our simulations were set equivalent to the experimental parameters with a silica sphere of diameter 15 nm and a density of surface silanol equal to 2.5 sites nm^{-2} (1790 titrating sites). The experimental value of the density of surface silanols was carefully validated [29] from the loss of ignition between 105 and 1100 °C and from the statistical cross-sectional area of water molecules adsorbed in the monolayer from the vapor phase. In our calculations, the dielectric permittivity value of silica has been set to 3.81. This value was obtained from Cauchy plot analysis [30]. In the present case the thickness, l_S, was equal to the radius of the experimental cation (sodium): 1.0 Å. The ionic concentration in the simulation was adjusted to 10^{-1}, 10^{-2}, and 10^{-3} mol L^{-1}, to mimic experimental ionic concentrations.

According to the Pauling principle of local neutralization of electric charge in ionic crystals, and due to the very low pK^0_{ai} of other reactions on the surfaces of silica particles [31], the charging behavior is expected to be fully dominated by the deprotonation of oxo groups according to

$$\text{Si–OH} \overset{K^0_a}{\rightleftarrows} \text{Si–O}^- + \text{H}^+. \tag{16}$$

The intrinsic pK^0_a value of this reaction was set to 7.6 according to the value obtained by Kobayashi et al. [32] and in agreement with calculated values obtained by Hiemstra et al. [33] ($pK^0_a = 7.5$). Equilibration times were obtained after 6000 Monte Carlo steps to obtain a representative statistical ensemble. The production time was then performed with 20,000 Monte Carlo steps. Equilibration and production times were achieved for each pH value. In Fig. 7 are presented the results corresponding to the homogeneous distribution. Since the exact surface site distribution was not available, both homogeneous and heterogeneous surface site distributions were considered. Similar results were obtained for homogeneous and heterogeneous distributions due to the low distance polydispersity index between sites of the heterogeneous site distribution. As expected, the surface charge density of silica is found to increase with increasing ionic concentration. As shown in Fig. 7, good agreement between the calculated and experimental charging process is obtained up to pH 8.0, i.e., before the dissolution

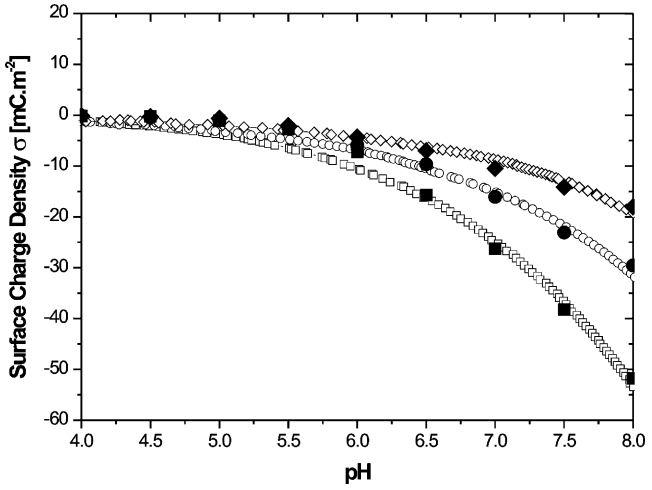

Fig. 7. Surface charge density, σ, of pyrogenic silica (the radius of the particle is equal to 7.5 nm with 1790 titrating sites), as a function of pH, at (◆) $C_i = 10^{-1}$, (●) 10^{-2}, and (■) 10^{-3} mol L^{-1} for experimental [29] (open symbols) and calculated titrating curves (filled symbols).

domain of silica [31]. Even if the model slightly underestimates the surface charge at low ionic strength and when the pH is close to the point of zero charge, without any fitting parameters, it correctly and quantitatively reproduces experimental data. This agreement is meaningful, since all parameters in the simulation model were used independent of any fitting parameters.

5. Summary

The influence of the surface site distribution and the importance of physicochemical conditions for the charging process of a NP were systematically investigated using a Grand Canonical Monte Carlo method. A Tanford and Kirkwood potential was used to consider spherical geometry and Coulomb interactions, as well as the salt effect and the presence of a dielectric discontinuity, and an explicit description of titrating sites was achieved. Because of this explicit description, comparisons between different spatial distributions of surface discrete sites (homogeneous, heterogeneous, and patch distributions) were possible, including ampholytic reaction equilibria. The present model shows that the distribution of sites plays an important role on

the charging process and points out the importance of complex competing interactions between Coulomb interactions, salt screening, and the reaction field due to the dielectric discontinuity between the NP and the solution.

It was found that ionic concentration decreases the intensity of the electrostatic interactions between charged sites and promotes the surface-charging process for all site distributions. It was shown that the total energy variations in patch distributions are different from those in homogeneous and heterogeneous distributions. For the patch distributions, charge depletion was observed at the center of the patch, since charges accumulate at the perimeter, where the charge density is lower. This finite size effect was found to decrease at high ionic concentration. For homogeneous and heterogeneous distributions, modifications of the NP dielectric has little effect on the NP surface charge density. At low dielectric NP constant, Coulomb interactions were found well counterbalanced by the reaction field. In contrast, patch distributions were more affected by ε_c variations. By increasing ε_c, the charging process was clearly promoted for all patch distributions due to the decrease of the importance of the Coulomb contribution. At low dielectric NP constant, the charging process was less effective due to the importance of the Coulomb electrostatic repulsions and presence of a reaction field that does not completely counterbalance them. Application of the present model to the pyrogenic silica charging process and comparisons with experimental data in the pH stability domain of pyrogenic silica at different ionic concentrations gave satisfactory results without using any fitting parameters.

This model represents a useful tool to understand the charging process of NPs by considering an explicit charging process of titrating sites and the complex interplay between Coulombic, salt, and reaction-field interactions. It could be extended to the study of multiple reaction sites (more than two), to heterogeneous distributions of pK_a, and to the charging behavior of NPs in concentrated solution to include the mutual influence of NPs. An explicit description of the ionic species in solution is now considered on the one hand, and on the other hand studies on the NP size effect, and comparison with other experimental data are also considered.

Acknowledgments

The authors are grateful to Professor G.S. Manning for stimulating discussions and personal communication, Dr. F. Thomas and Dr. B. Prélot for kindly providing experimental data, and Professor M. Borkovec, Dr. P.-Y. Morgantini, F. Avaltroni, and F. Cerveau for their help and encouragement. We gratefully acknowledge the financial support received from the Swiss National Science Foundation, Project 200020-101974/1.

References

[1] W. Stumm, J.J. Morgan, Aquatic Chemistry: Chemical Equilibria and Rates in Natural Waters, third ed., Wiley, New York, 1996.
[2] S. Ulrich, A. Laguecir, S. Stoll, J. Nanopart. Res. 6 (2004) 595–603.
[3] I.C. Bourg, G. Sposito, A.C.M. Bourg, J. Colloid Interface Sci. 312 (2007) 297–310.
[4] J.A. Davis, R.O. James, J.O. Leckie, J. Colloid Interface Sci. 63 (1978) 480–499.
[5] T. Hiemstra, W.H. Van Riemsdijk, G.H. Bolt, J. Colloid Interface Sci. 133 (1989) 91–104.
[6] T. Hiemstra, W.H. van Riemsdijk, J. Colloid Interface Sci. 179 (1996) 488–508.
[7] P. Zarzycki, Langmuir 22 (2006) 11234–11240.
[8] M. Seijo, S. Ulrich, M. Filella, J. Buffle, S. Stoll, Phys. Chem. Chem. Phys. 8 (2006) 5679–5688.
[9] M. Borkovec, Langmuir 13 (1997) 2608–2613.
[10] F.H. Stillinger Jr., J. Chem. Phys. 35 (1961) 1584–1589.
[11] R.R. Netz, J. Phys. Condens. Matter 15 (2003) S239–S244.
[12] C. Tanford, J.G. Kirkwood, J. Am. Chem. Soc. 79 (1957) 5333–5339.
[13] C. Tanford, Physical Chemistry of Macromolecules, Wiley, New York, 1963.
[14] W.H. Orttung, J. Phys. Chem. 72 (1968) 4066–4071.
[15] W.H. Orttung, Nature 220 (1968) 1122–1124.
[16] F.L. da Silva, B. Jonsson, R. Penfold, Protein Sci. 10 (2001) 1415–1425.
[17] A. Warshel, S.T. Russell, Q. Rev. Biophys. 17 (1984) 283–422.
[18] J.J. Havranek, P.B. Harbury, Proc. Natl. Acad. Sci. USA 96 (1999) 11145–11150.
[19] Y.H. Kao, C.A. Fitch, S. Bhattacharya, C.J. Sarkisian, J.T. Lecomte, E.B. Garcia-Moreno, Biophys. J. 79 (2000) 1637–1654.
[20] P. Linse, J. Phys. Chem. 90 (1986) 6821–6828.
[21] N. Metropolis, A.W. Rosenbluth, M.N. Rosenbluth, A.H. Teller, E. Teller, J. Chem. Phys. 21 (1953) 1087–1092.
[22] L.J. Henderson, Am. J. Physiol. 21 (1908) 427–448.
[23] K.A. Hasselbalch, Biochem. Z. 78 (1916) 112–114.
[24] P. Zarzycki, J. Colloid Interface Sci. 297 (2006) 204–214.
[25] P. Szabelski, P. Zarzycki, R. Charmas, Langmuir 20 (2004) 997–1002.
[26] G.S. Manning, Macromolecules 40 (2007) 8071–8081.
[27] G.S. Manning, J. Phys. Chem. B 111 (2007) 8554–8559.
[28] M.K. Gilson, B.H. Honig, Proteins Struct. Funct. Genet. 3 (1988) 32–52.
[29] B. Prelot, W. Janusz, F. Thomas, F. Villieras, R. Charmas, W. Piasecki, W. Rudzinski, Appl. Surf. Sci. 196 (2002) 322–330.
[30] D.B. Hough, L.R. White, Adv. Colloid Interface Sci. 14 (1980) 3–41.
[31] R.K. Iler, The Chemistry of Silica: Solubility, Polymerization, Colloid and Surface Properties and Biochemistry, Wiley, New York, 1979.
[32] M. Kobayashi, F. Juillerat, P. Galletto, P. Bowen, M. Borkovec, Langmuir 21 (2005) 5761–5769.
[33] T. Hiemstra, J.C.M. De Wit, W.H. Van Riemsdijk, J. Colloid Interface Sci. 133 (1989) 105–117.